Particle size studies of supported metal catalysts: a comparative study by X-ray diffraction, EXAFS and electron microscopy

A.T. Ashcroft [a], A.K. Cheetham [a,1], P.J.F. Harris [b], R.H. Jones [c,d], S. Natarajan [c], G. Sankar [c], N.J. Stedman [b] and J.M. Thomas [c,1]

[a] *Materials Department, University of California, Santa Barbara, CA 93106, USA*
[b] *Chemical Crystallography Laboratory, 9 Parks Road, Oxford OX1 3PD, UK*
[c] *Davy Faraday Laboratory, Royal Institution, 21 Albemarle St., London W1 4BX, UK*
[d] *Department of Chemistry, University of Keele, Keele, Staffordshire ST5 5BG, UK*

Received 12 July 1993; accepted 15 October 1993

Supported ruthenium and iridium metal catalysts are studied by X-ray diffraction (XRD), EXAFS analysis and transmission electron microscopy (TEM). Estimates of the mean particle size from these techniques range from 20 to 25 Å from XRD, 13 to 16 Å from EXAFS and 25 to 32 Å from TEM. The strengths and weaknesses of these instrumental methods are discussed, as is the intrinsic comparability of these techniques. From a combination of these methods, the average particle size is estimated to be of the order of 20–30 Å.

Keywords: Particle size; X-ray diffraction; electron microscopy; EXAFS; catalysts

1. Introduction

It has previously been shown [1,2] that supported ruthenium and iridium metals are excellent catalysts for the dry reforming of methane and carbon dioxide to synthesis gas according to

$$CH_4 + CO_2 \rightarrow 2CO + 2H_2 \quad (1)$$

and that rare-earth iridium- and ruthenium-containing pyrochlores decompose under reaction conditions to produce an active iridium or ruthenium species [3]. Previously, a number of methods have been used to estimate particle sizes. Examples include the use of X-ray diffraction (XRD) [4] and transmission electron microscopy (TEM) [5] to study zirconia, the use of XRD [6] to study iron oxide based catalysts, and the use of TEM and gas adsorption to study ruthenium on car-

[1] To whom correspondence should be addressed.

bon [7]. A comprehensive study of sulphated metal oxide catalysts using a variety of techniques, including electron microscopy and XRD, has also been performed [8]. EXAFS analysis has been used to estimate particle sizes of supported copper catalysts, either by a comparison of reductions in coordination numbers [9,10], or by observing a contraction in the nearest-neighbour metal–metal distances [11].

In this work, we compare estimates of the size of supported catalyst particles determined from XRD, EXAFS analysis and TEM. In addition to bright field imaging, some high resolution lattice images were recorded. The accuracy and limitations of each technique are also discussed.

2. Experimental

The preparation of the rare-earth iridium- and ruthenium-containing pyrochlores has been described previously [12]. The materials studied by XRD were reduced during in situ XRD studies [13]. Samples of europium iridate, $Eu_2Ir_2O_7$, and gadolinium ruthenate, $Gd_2Ru_2O_7$, mixed with silica were utilised as catalysts for the production of syngas from methane via dry-reforming (both catalysts) and via partial oxidation (the iridate only). Experiments were performed at temperatures of up to 1013 K, and the catalysts cooled to room temperature before diffraction patterns were recorded using a Siemens D500 diffractometer with a Stoe rotating anode X-ray source. The samples studied by TEM and EXAFS were reduced in an in situ energy dispersive XRD study [3] under the dry-reforming gas mixture. The pyrochlore catalysts were mixed with silica and heated at a rate of 50 K/min under a mixture of 25% CH_4, 25% CO_2, 50% Ar to 1100 K. Once the XRD pattern showed no trace of the pyrochlore peaks, the sample was allowed to cool under the gas mixture before it was removed for further study.

For the TEM measurements, a few drops of chloroform were added to a few, finely ground, grains of the compound and the resultant suspension sonicated in an ultrasound bath. One drop of the suspension was then pipetted on to a 3 mm copper grid coated with a holey, carbon-dusted, Formvar (polyvinylformal) film. Bright field micrographs were recorded at accelerating voltages of 200 kV using a Jeol 2000FX instrument and at 400 kV using a Jeol 4000EX instrument. Lattice images were recorded on the Jeol 4000EX microscope (resolution approximately 1.7 Å) using an objective aperture large enough to allow the ruthenium 100 and 002 reflections to pass through.

For the EXAFS study, data were collected in transmission on Station 9.2 at Daresbury Laboratory. Station 9.2, with an order-sorting double-crystal Si(220) monochromator, is on the 5T wiggler beam line and has usable intensity available at the high energies (ca. 22 keV) required to study the ruthenium K edge. In all cases, transmission measurements were performed using two ionisation chambers with appropriate gas mixtures in order to monitor the incident and transmitted beam intensities. Samples were diluted with boron nitride, finely ground, and stuck

to a sample holder using Sellotape. Samples of rare-earth oxides, ruthenium dioxide and ruthenium metal powder were also run as standards.

3. Results

The results from different techniques will be presented in the following sections and then discussed together.

3.1. X-RAY DIFFRACTION (XRD)

Particle size estimates were obtained by fitting a pseudo-Voigt function to the iridium 111 reflection and to the ruthenium 002 reflection. The angle, θ, at which the peak maximum occurred, full width at half the maximum intensity, B, and the wavelength, λ, of the copper radiation were then inserted into the Scherrer equation, $t = 0.9\lambda/B\cos\theta$ [14], to obtain estimates of the sample thickness, t, which we have equated with the particle size. The results are shown in table 1 and a typical profile fitting is shown in fig. 1.

3.2. EXAFS ANALYSIS

The ruthenium K-edge data were processed using the suite of programs available at Daresbury Laboratory: EXCALIB to convert the raw data into electron-volts, EXBROOK for pre-edge subtraction, normalisation and background subtraction, and EXCURV90 for curve-fitting analysis of the EXAFS data. The analysis was performed using the curved-wave and single-scattering theory options in the EXCURV90 program. Ruthenium metal powder (Aldrich Chemical Company) was used as a standard to estimate the phase-shift and amplitude information, using coordination shell information obtained from the Inorganic Crystal Structure Database (ICSD) located at Daresbury Laboratory. Ruthenium metal adopts a hexagonal close packed structure, so the central atom has two shells of six atoms at distances of 2.67 and 2.72 Å, respectively. Because of the close proximity of these two shells, the peaks arising from them in Fourier transforms overlap completely. For simplicity, the two shells were treated as a single shell of twelve ruthe-

Table 1
Particle size estimates obtained by fitting pseudo-Voigt functions to XRD patterns

Sample	Reaction [a]	Formation temperature (K)	Particle size (Å)
used $Eu_2Ir_2O_7$	a	993	25
used $Eu_2Ir_2O_7$	b	873	25
used $Gd_2Ru_2O_7$	a	1013	20

[a] a = dry-reforming, b = partial oxidation.

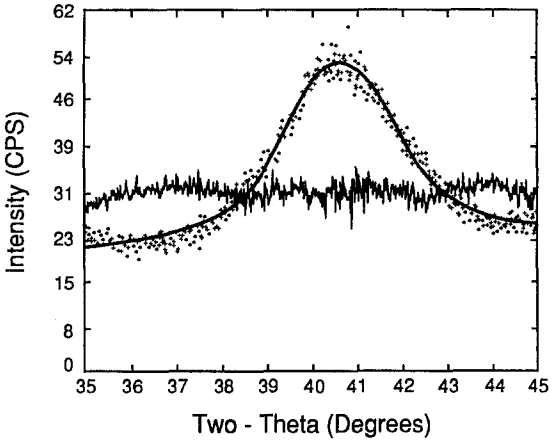

Fig. 1. A pseudo-Voigt function fitted to the (111) reflection of iridium metal; crosses show the experimental data and a smooth curve indicates the fitted function; a difference curve is also shown.

nium atoms at 2.695 Å during data analysis. The first peak in the radial distribution function, representing this first ruthenium coordination shell, was Fourier filtered out using limits of 1.69 and 3.09 Å, and analyzed to obtain the structural parameters.

The results of curve-fitting analyses for four rare-earth ruthenates that had decomposed during catalysis of the partial oxidation reaction are shown in table 2, and a comparison of experimentally derived and calculated Fourier transforms and EXAFS $k^3\chi(k)$ functions for ruthenium powder and the decomposed europium ruthenate are shown in fig. 2. It can be seen that the apparent coordination numbers were all found to be less than the bulk coordination of twelve, indicating the presence of relatively small particles. The average ruthenium–ruthenium distances are slightly lower than the expected 2.695 Å, which is consistent with the smaller coordination number obtained from the analysis, since it is known that the lattice parameters are contracted for small metal particles [15]. Assuming that the particles are spherical, approximate sizes may be estimated using the method of Greegor and Lytle [16]. This is more rigorous than the treatment described in ref.

Table 2
Results of EXAFS analysis for various reduced rare-earth ruthenates

Sample	Coord. No.	M–M distance (Å)	$\Delta\sigma^2$	Calc. diameter (Å)
Ru powder	12.0	2.695	–	–
used $Eu_2Ru_2O_7$	10.07	2.688	0.00129	16
used $Gd_2Ru_2O_7$	9.67	2.685	0.00160	14
used $Nd_2Ru_2O_7$	9.63	2.683	0.00168	14
used $Sm_2Ru_2O_7$	9.36	2.685	0.00212	13

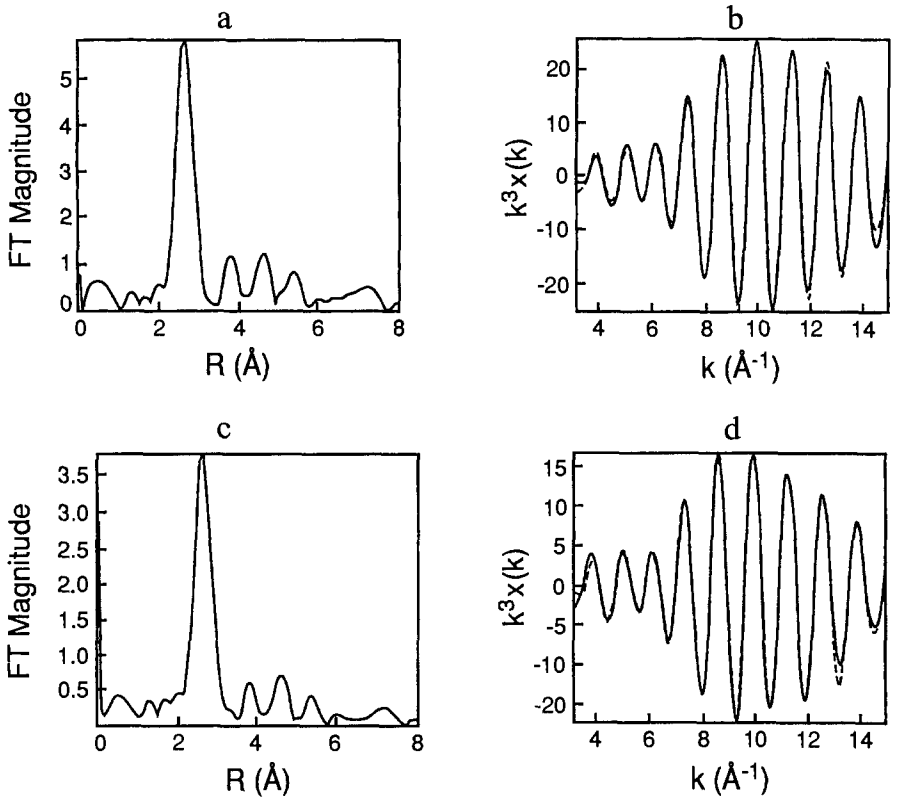

Fig. 2. Experimentally derived (solid lines) and calculated (broken lines) Fourier transforms and EXAFS $k^3\chi(k)$ functions of ruthenium powder (a, b), and reduced $Eu_2Ru_2O_7$ (c, d). Similar fits were obtained for $Gd_2Ru_2O_7$, $Nd_2Ru_2O_7$ and $Sm_2Ru_2O_7$.

[2], where ruthenium particles with similar coordination numbers were assumed to be of 30 Å or larger.

3.3. BRIGHT FIELD IMAGING

In bright field imaging, any crystalline material of sufficient thickness (approximately 6 Å in the present case) should appear as a dark area on the image. By obtaining numerous micrographs of a number of ruthenates and the neodymium iridate after catalysis, and measuring the particles, a particle size distribution for each compound was obtained. For each sample, at least eight micrographs were taken on the Jeol 2000FX instrument. Distinct particles were measured and classified as approximately 1, 2, 3, 4 or 5 mm on the print. These sizes were then divided by the reproduction enlargement factor and the magnification to obtain the approximate sizes in ångstroms. The histograms of particle size distribution are shown in fig. 3, and the results summarised in table 3, where it can be seen that the average particle sizes and distributions are similar for all four of the ruthenates.

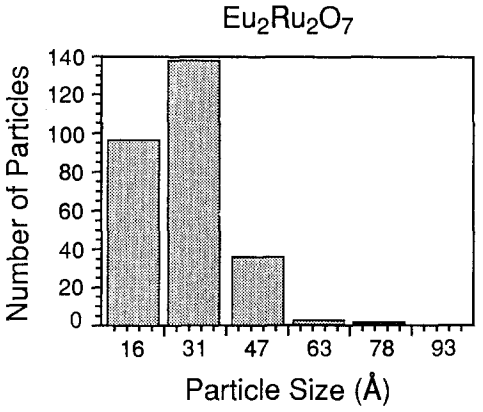

Fig. 3. Histogram showing a particle size distribution for a reduced $Eu_2Ru_2O_7$ catalyst, as obtained by bright field imaging at a magnification of ×330 000.

In order to see whether a microscope with higher resolution and a higher accelerating voltage (hence capable of penetrating thicker regions) could allow smaller particles to be distinguished, the neodymium and samarium ruthenates were also studied at 400 kV. A micrograph of neodymium ruthenate is shown in fig. 4, the particle size distributions are illustrated in fig. 5 and the data are summarised in table 4.

3.4. HIGH RESOLUTION TEM (HRTEM)

A typical HRTEM micrograph of reduced samarium ruthenate is shown in fig. 6, where fringes may readily be observed. The region labelled A contains lattice fringes, the spacings of which may be measured as 2.14 Å, which correspond to the 002 planes in ruthenium metal. The regions marked B and C have lattice fringes which are 2.33 Å apart, which correspond to the 100 planes of ruthenium metal. These particles appear to be of the order of 30–40 Å, but only the lattice fringes

Table 3
Particle sizes for various ruthenates and neodymium iridate after use in the catalytic reactor, obtained using the Jeol 2000FX microscope operating at ×330 000 magnification

Sample	% particles of size						Mean size (Å)
	16 Å	31 Å	47 Å	63 Å	78 Å	93 Å	
used $Eu_2Ru_2O_7$	35	51	13	1	0	0	28.2(6)
used $Gd_2Ru_2O_7$	22	52	24	2	0	0	32(1)
used $Nd_2Ru_2O_7$	28	57	13	2	1	0	30.0(9)
used $Sm_2Ru_2O_7$	34	50	13	2	0	1	29.2(8)
used $Nd_2Ir_2O_7$	40	55	5	0	0	0	25.8(6)

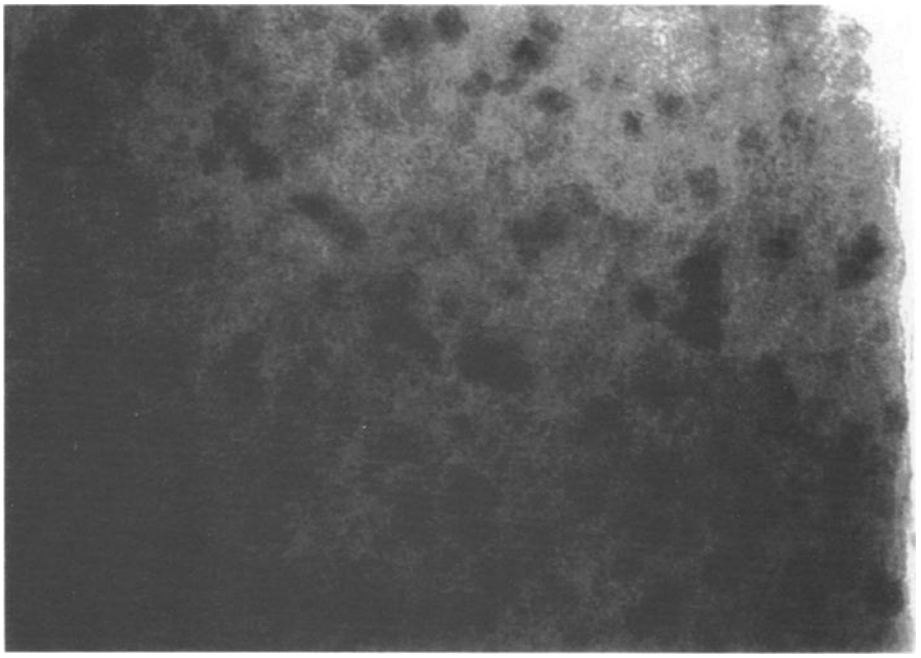

Fig. 4. Electron micrograph of reduced europium ruthenate recorded at a magnification of ×385 000.

from larger particles are likely to be observable since contrast from very small particles would be obscured by contrast from the support. Moreover, only particles in certain orientations will be visible by lattice imaging.

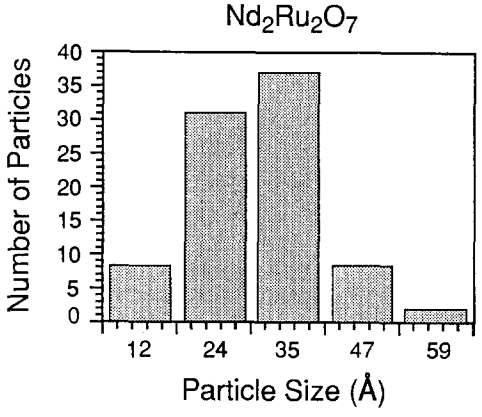

Fig. 5. Histogram showing a particle size distribution for reduced neodymium ruthenate after use in the catalytic reactor, as obtained by bright field imaging at a magnification of ×385 000.

Table 4
Particle sizes for neodymium and samarium ruthenates after use in the catalytic reactor, obtained using the Jeol 4000EX microscope operating at ×385 000 magnification

Sample	% particles of size					Mean size (Å)
	12 Å	24 Å	35 Å	47 Å	59 Å	
used $Nd_2Ru_2O_7$	9	35	42	10	3	31(1.1)
used $Sm_2Ru_2O_7$	11	41	39	9	0	29(1.3)

4. Discussion

The various techniques used in this study have intrinsic strengths and weaknesses. X-ray diffraction is phase specific, unless impurities have diffraction peaks in the area of study, which was less of a problem for the Ir 111 peak than for the Ru 002. The figure obtained by XRD comes from measurement of a single peak-width and is likely to be influenced by strain within the crystallites. Also, very small particles are likely to produce diffraction peaks which are too broad to be observed. It should be noted that XRD gives no indication of the range of particle sizes present in the sample.

EXAFS is not phase-specific, but is element specific. The use of EXAFS analysis to obtain particle sizes is regarded as fairly crude [17] and the figures of less than 20 Å obtained from EXAFS analysis are likely to underestimate the average particle size. This method is based upon the average coordination number of the ruthenium atoms, and there will be a contribution to this from unreduced ruthenium atoms which will appear to have a much lower FT magnitude at 2.7 Å, thereby reducing the apparent coordination number of the ruthenium shell. It has also been argued that anharmonic effects in small particles can lead to an underestimate of coordination numbers by EXAFS [18]. The presence of defects will also reduce the average coordination number, again leading to an underestimate. Furthermore, size estimates from this method are very sensitive to the assumed particle shape, and a higher estimate would be obtained if a morphology with a higher surface to volume ratio (e.g. disk) was chosen [16]. As with XRD, the EXAFS method is insensitive to the range of particle sizes.

Electron microscopy is neither element nor phase specific, but provides a much more direct measure of particle sizes. Unlike the other methods, it does enable us to probe the particle size distribution. On the other hand, there are a number of reasons why particle size estimates from microscopy may not be accurate. A major problem is that it only involves the study of a relatively small proportion of the whole material, and it is always possible that the crystallites which are studied by this technique are not representative of the sample as a whole. Secondly, bright field imaging has proved very useful for measuring particle size distributions where heavy metals are supported on light element carriers such as alumina [19], but it is

Fig. 6. HRTEM micrograph of reduced samarium ruthenate recorded at a magnification of ×385000.

somewhat more difficult to apply where strongly scattering supports are used, as in the present study. The relatively poor contrast between metal particles and the support may lead to smaller metal particles being obscured, thus resulting in an overestimate of mean particle size. Thirdly, it is difficult to tell whether large particles are, in fact, two or more smaller particles which are close together. Fourthly, it is possible that particles forming below the surface or away from the edge of the sample may be smaller because their growth is hindered. These particles may not be observable by this method as they are hidden by larger particles growing above them, or are in regions of the sample which are too thick to view properly. Finally, measuring and classifying large numbers of particles is very laborious, and human error may also be significant. Using a higher resolution microscope provided data which were similar to those obtained previously, and so the greater resolution and accelerating voltage do not appear to make a difference. This method appears to be reproducible, as a completely different set of crystallites was studied, but may over-estimate the actual average particle size due to difficulties in observing the smallest particles.

Even allowing for the limitations of each method, as discussed above, it is possible that the results may not be truly comparable because of intrinsic differences between the techniques. EXAFS is produced by interactions between out-going core electrons and the electron density of neighbouring atoms, and involves a calculation based upon interatomic distances and coordination numbers that may lead to a slightly lower estimate of particle size for very small particles. XRD involves the whole of the electron density, while TEM measures the projected atomic potentials from the particles, which will appear larger than the electron density. Indeed, the projection itself may overestimate the size. Taking these caveats into account, the agreement between the different estimates in the present work is rather good and these are consistent with a mean particle size of approximately 25 Å.

Acknowledgement

We thank the SERC, Amoco and BP for financial support. This work was also supported by the MRL Program of the National Science Foundation under Award No. DMR-9123048. ATA would like to thank British Gas for a CASE award, and RHJ thanks the Royal Society for a Warren Fellowship. The authors wish to thank Professor J.S. Speck and Dr. A.P. Wilkinson for useful discussions, Professor G.N. Greaves and Drs. J.L. Hutchison and P.D. Battle for helpful advice, and Dr. J.W. Couves and J.J. Owen for experimental assistance.

References

[1] A.T. Ashcroft, A.K. Cheetham, M.L.H. Green and P.D.F. Vernon, Nature 352 (1991) 225.

[2] J.S.H.Q. Perera, J.W. Couves, G. Sankar and J.M. Thomas, Catal. Lett. 11 (1991) 219.
[3] A.T. Ashcroft, A.K. Cheetham, R.H. Jones, S. Natarajan, J.M. Thomas, D. Waller and S.M. Clark, J. Phys. Chem. 97 (1993) 3355.
[4] R. Srinivasan and R. De Angelis, J. Mater. Res. 1 (1986) 583.
[5] R. Srinivasan, L. Rice and B.H. Davis, J. Am. Ceram. Soc. 73 (1990) 3528.
[6] M.M. Ibrahim, J. Zhao and M.S. Seehra, J. Mater. Res. 7 (1992) 1856.
[7] S. Galvagno, G. Capannelli, G. Neri, A. Donato and R. Pietropaolo, J. Mol. Catal. 64 (1991) 237.
[8] V.R. Pradhan, J.W. Tierney and I. Wender, Energy and Fuels 5 (1991) 497.
[9] B.S. Clausen and H. Topsøe, Catal. Today 9 (1991) 189.
[10] G. Sankar, J.M. Thomas, D. Waller, J.W. Couves, C.R.A. Catlow and G.N. Greaves, J. Phys. Chem. 96 (1992) 7485.
[11] G. Apai, J.F. Hamilton, J. Stohr and A. Thompson, Phys. Rev. Lett. 43 (1979) 165.
[12] R.H. Jones, A.T. Ashcroft, D. Waller, A.K. Cheetham and J.M. Thomas, Catal. Lett. 8 (1991) 169.
[13] A.T. Ashcroft, A.K. Cheetham, R.H. Jones, S. Natarajan, J.M. Thomas and D. Waller, *Catalysis and Surface Characterisation*, Special Publ. Roy. Soc. Chem. 114 (1992) 184.
[14] A.R. Stokes and A.J.C. Wilson, Proc. Camb. Phil. Soc. 38 (1942) 313.
[15] M. Che and C.O. Bennett, Adv. Catal. 36 (1989) 55.
[16] R.B. Greegor and F.W. Lytle, J. Catal. 63 (1980) 476.
[17] P.A. Lee, P.H. Citrin, P. Eisenberger and B.M. Kincaid, Rev. Mod. Phys. 53 (1981) 769.
[18] B.S. Clausen, L. Grabaek, H. Topsøe, L.B. Hansen, P. Stoltze and J.K. Norskov, J. Catal. 141 (1993) 368.
[19] P.J.F. Harris, E.D. Boyes and J.A. Cairns, J. Catal. 82 (1983) 127.